Systematic Study on the Effect of Solvent Removal Rate on the Morphology of Solvent Vapor Annealed ABA Triblock Copolymer Thin Films

Julie N. L. Albert, Wen-Shiue Young, Ronald L. Lewis, III, Timothy D. Bogart, Jasmine R. Smith, and Thomas H. Epps, III*

Chemical Engineering Department, University of Delaware, Newark, Delaware 19716, United States

ABSTRACT

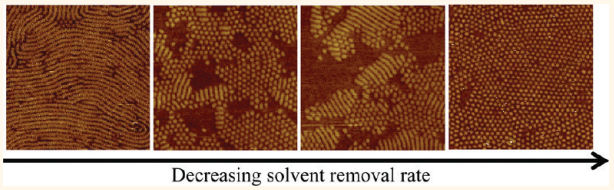

Nanoscale self-assembly of block copolymer thin films has garnered significant research interest for nanotemplate design and membrane applications. To fulfill these roles, control of thin film morphology and orientation is critical. Solvent vapor annealing (SVA) treatments can be used to kinetically trap morphologies in thin films not achievable by traditional thermal treatments, but many variables affect the outcome of SVA, including solvent choice, total solvent concentration/swollen film thickness, and solvent removal rate. In this work, we systematically examined the effect of solvent removal rate on the final thin film morphology of a cylinder-forming ABA triblock copolymer. By kinetically trapping the film morphologies at key points during the solvent removal process and then using successive ultraviolet ozone (UVO) etching steps followed by atomic force microscopy (AFM) imaging to examine the through-film morphologies of the films, we determined that the mechanism for cylinder reorientation from substrate-parallel to substrate-perpendicular involved the propagation of changes at the free surface through the film toward the substrate as a front. The degree of reorientation increased with successively slower solvent removal rates. Furthermore, the AFM/UVO etching scheme permitted facile real-space analysis of the thin film internal structure in comparison to cross-sectional transmission electron microscopy.

KEYWORDS: solvent annealing · solvent removal · block copolymer · thin film · self-assembly · morphology · orientation

Block copolymer self-assembly in thin film geometries (~100 nm thickness) has garnered significant interest due to the potential applications of copolymer materials as nanotemplates,[1−3] nanoporous membranes,[4−7] active layers in organic optoelectronics,[8] and antireflection coatings.[9] In AB diblock and ABA triblock copolymer systems, self-assembly is primarily controlled by the block interactions (interaction parameter, χ), number of segments per polymer chain (N), and block volume fractions (f).[10,11] Common morphologies include spheres, cylinders, gyroid network, and lamellae, which have periodicities, or domain spacings (L_0), on the order of 10−100 nm.[10] However, compared to bulk materials, thin film self-assembly is strongly influenced by commensurability considerations (ratio of film thickness to domain spacing) and surface energetics (free surface and substrate surface energies).[12] Additionally, nanostructure orientation relative to a substrate surface is a critical consideration for many of the above-mentioned applications.[12]

Traditionally, solvent vapor annealing (SVA) has been used as an alternative to thermal annealing for copolymers that are susceptible to thermal transitions or degradation.[13−15] However, it also is attractive as a general approach for controlling thin film self-assembly for several additional reasons. First, the selectivity of the solvent vapor can create an effectively neutral free surface[16,17] or a surface that preferentially attracts the higher surface tension block by reducing preferential segregation of the lower surface tension block to the free surface. Second, vapor sorption into the film promotes self-assembly by lowering the glass transition temperature of each block, increasing chain mobility.[14,16,18] Third, vapor sorption affects block interactions, block volume fractions, and nanostructure domain spacing, which can lead to mitigation of substrate surface preferences, induce changes in morphology, and/or impact commensurability considerations.[14,16,19−23]

SVA results are affected by solvent choice, total solvent concentration (which dictates swollen film thickness), and solvent removal

* Address correspondence to thepps@udel.edu.

Received for review October 3, 2011 and accepted November 28, 2011.

Published online December 09, 2011
10.1021/nn203776c

rate. The latter parameter is instrumental in kinetically trapping desirable morphologies or nanostructure orientations.[3,24−26] Instantaneous solvent removal is typically employed in SVA experiments to trap the morphologies present in swollen films; however, the nanostructure lattice symmetry can become distorted upon solvent removal.[27] In contrast, slower solvent removal during film casting or after SVA can produce intriguing morphologies. Kim and Libera reported one of the first studies on the effects of solvent removal rate in block copolymer thin films.[28] They examined cylinder-forming poly(styrene-*b*-butadiene-*b*-styrene) (SBS) films cast from toluene and showed that poor ordering was obtained for very fast solvent removal. Using successively slower solvent removal rates, improved ordering was noted, with a transition from cylinders oriented perpendicular to the substrate, to mixed orientations, and finally to cylinders oriented parallel to the substrate.[28] Recent work by Phillip *et al.* noted similar behavior.[25] Additionally, Fukunaga *et al.* found that lamellar triblock copolymer films oriented perpendicular to the substrate for fast solvent removal rates and parallel to the substrate for slow solvent removal rates.[29]

However, findings by Elbs *et al.* showed that the role of solvent removal rate is more complex.[30] In that work, the triblock copolymer morphologies identified as a function of solvent removal rate included a poorly ordered "micellar" phase, a "wagon-wheel" pattern indicative of a bicontinuous gyroid network, and a mixture of structures at the film surface, including core−shell cylinders, spheres in cylinders, and helices around cylindrical cores.[30] Thus, manipulation of solvent removal rate has the potential to produce unique thin film morphologies, but its true effect on nanostructure formation (and orientation) is poorly understood. In order to gain insight into the reordering mechanism associated with solvent removal, in our study, we kinetically trapped the film morphologies (*via* instantaneous solvent removal) at key points during the SVA process and then employed a creative film etching scheme to image the through-film morphology more easily and quickly than is possible with cross-sectional transmission electron microscopy (TEM). This simple scheme utilized successive ultraviolet ozone (UVO) etching steps followed by atomic force microscopy (AFM) imaging.

We examined both the effect of solvent removal rate on the final morphology and the morphology development during the solvent removal process. Films were characterized after complete solvent removal (identified by a return to the original film thickness) using AFM combined with a thin film peeling technique that enabled characterization of the film morphology adjacent to the substrate,[31,32] successive UVO etching steps as previously described, and cross-sectional TEM to validate the AFM/UVO etching approach. By manipulating the solvent removal rate and examining the morphology development over time, we followed the reorientation of cylindrical morphologies, and we showed that the

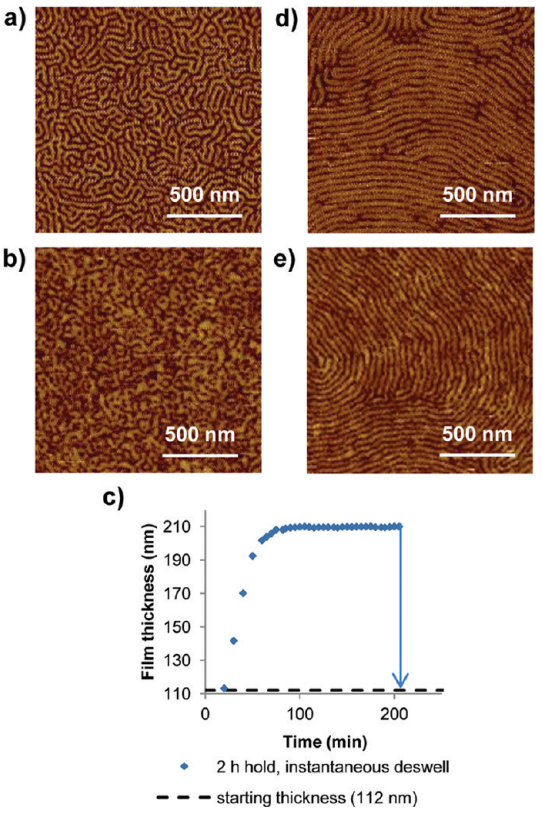

Figure 1. (a) AFM phase image of the free surface of the as-cast dS-l-dS film. (b) AFM phase image of the as-cast dS-l-dS film adjacent to the substrate surface. (c) Film thickness profile for dS-l-dS film annealed with chloroform vapor and held at a constant swollen thickness for 2 h prior to instantaneous (<10 s) removal of solvent from the film. (d) AFM phase image of the free surface of the film annealed with the profile in (c). (e) AFM phase image of the film adjacent to the substrate surface for the film annealed with the profile in (c).

mechanism for this cylinder reorientation involved the propagation of changes from the free surface through the film and toward the substrate as a front.

RESULTS AND DISCUSSION

Thin films of a cylinder-forming poly(deuterated styrene-*b*-isoprene-*b*-deuterated styrene) (dS-l-dS; number average molar mass M_n = 160 kg/mol; volume fractions f_{dS} = 0.10, f_I = 0.78, f_{dS} = 0.12; domain spacing L_0 = 37 nm) were flow coated[33] onto UVO-cleaned silicon substrates. After casting, the films were annealed with chloroform vapor, and the swollen film thickness was monitored and controlled *in situ*. All films were initially swollen to 208 ± 3 nm (5.6 × L_0, 46 vol % solvent in the film) and held for 2 h prior to solvent removal. Solvent removal rates investigated included instantaneous (<10 s) solvent removal and deswell rates of 0.5, 0.1, and 0.05 nm/min. For noninstantaneous solvent removal rates, the remaining solvent was instantaneously removed from the film at 125 nm (3.4 × L_0, 10% solvent). (Note: 10% solvent content is well below the solvent concentration required to raise the glass transition of PS above 25 °C, thus the morphology would not have continued to evolve.)[34]

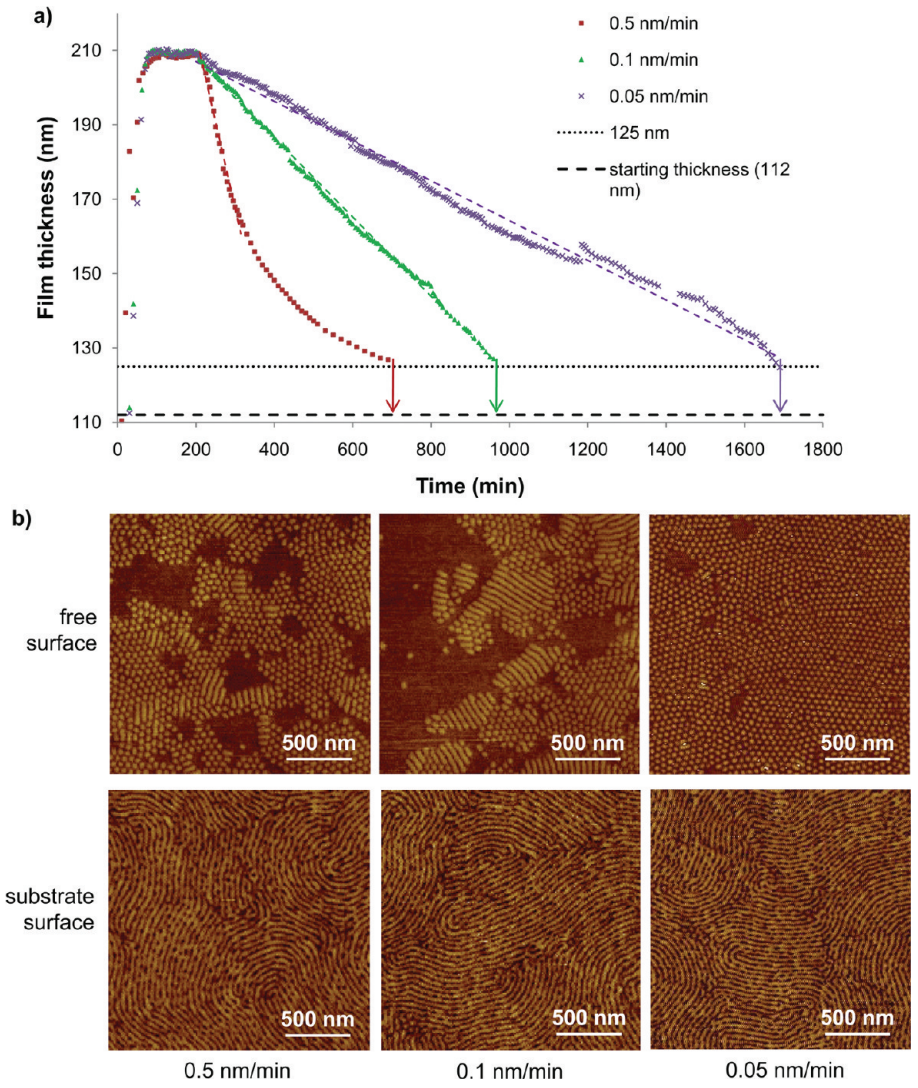

Figure 2. Comparison of solvent removal rates and corresponding morphologies. (a) Film thickness profiles for films annealed with chloroform vapor at a constant swollen thickness for 2 h followed by different solvent removal profiles/rates. For the nonlinear profile (red squares), the initial deswell rate was 0.5 nm/min (slope corresponding to the first 100 min of solvent removal). (b) AFM phase images of the films corresponding to the annealing profiles in (a) at the free surface (top panels) and the substrate surface (bottom panels).

As-Cast and Instantaneous Solvent Removal Morphologies. The as-cast films were 112 ± 2 nm (3.0 × L_0) thick and had a poorly ordered morphology, as fast solvent evaporation during casting limited film ordering (see Figure 1a,b). Upon instantaneous solvent removal from a film swollen to 208 nm, the swollen film morphology was trapped, and parallel cylinders were identified at both the free surface and the substrate surface (see Figure 1c–e). The parallel cylinder orientation was expected, as both the substrate and the free surface are preferential for the PI block;[35] chloroform is only slightly selective for dPS and therefore would not be expected to mitigate these surface preferences except at very high solvent concentrations. Knoll *et al.* showed that SBS films annealed with chloroform showed only parallel orientations for films thicker than 3 × L_0 and chloroform vapor pressures $p/p_0 > 0.65$, where p is the vapor pressure of chloroform in the annealing chamber and p_0 is the saturated vapor pressure at 25 °C, criteria that our annealing conditions met.[19]

Morphology as a Function of Solvent Removal Rate. The film thickness profiles and AFM images of films subjected to slower deswell rates (0.5, 0.1, 0.05 nm/min) are presented in Figure 2. The slowest solvent removal rate had the most uniform top surface, with a hexagonally packed structure, corresponding to perpendicular cylinders based on the bulk morphology, whereas faster rates contained mixed regions of perpendicular cylinders, parallel cylinders, and featureless areas. The fractions of each morphology type at each solvent removal rate are summarized in Table 1. Aside from disruption of the surface parallel nanostructure, no obvious correlations between morphology and solvent removal rate existed, though comparison of the instantaneous rate

TABLE 1. Characterization of Morphologies for Different Deswell Rates Based on Statistics Calculated from AFM Images Corresponding to the Following Numbers of Samples for Each Deswell Rate: Instantaneous, 3 samples; 0.5 nm/min, 2 samples; 0.1 nm/min, 2 samples; 0.05 nm/min, 1 sample

solvent removal rate	fraction perpendicular cylinders	fraction parallel cylinders	fraction featureless
instantaneous	0.02 ± 0.01	0.98 ± 0.01	0.0 ± 0.0
0.5 nm/min	0.71 ± 0.05	0.12 ± 0.04	0.17 ± 0.02
0.1 nm/min	0.47 ± 0.11	0.20 ± 0.11	0.34 ± 0.04
0.05 nm/min	0.94 ± 0.01	0.02 ± 0.01	0.04 ± 0.01

(Figure 1d,e) and the slowest rate (Figure 2b) suggested that slower rates would give rise to more perpendicular structures. Interestingly, the morphologies of the films at the substrate surface were all similar to the original swollen film parallel cylinder morphology, except that the PI domains appear to be perforated by dPS domains. This result suggested that the rearrangement at the free surface upon slow solvent removal did not propagate through the entire film thickness.

Additionally, fast Fourier transforms (FFTs) of the AFM images in Figures 1 and 2 revealed that the domain sizes were nearly identical at the free surfaces of all annealed films, and that the domain sizes at the substrate surfaces were smaller in all cases. The domain size at the substrate surface coincided with the domain size of the as-cast (unannealed) sample instead of the domain size at the free surface (see Figure S1 in the Supporting Information). These findings suggest that, during SVA, chains in contact with the substrate surface were effectively pinned and unable to swell to the same degree as their through-film and free surface counterparts. As a result, the polymer chains adjacent to the substrate surface experienced insufficient swelling to mitigate substrate surface preferences. Furthermore, the kinetics of reordering during solvent removal would have been significantly slower adjacent to the substrate compared with the remainder of the film, which explains the minimal changes noted in the film morphology at the substrate interface during the solvent removal treatments.

Through-Film Morphology. In order to more closely examine the propagation of the free surface morphology through the film, we employed successive AFM/UVO etching steps. For the 0.5 nm/min rate (see Figure 3a), the transition between the free surface morphology (hexagonally packed structures, parallel cylinders, featureless areas) and the substrate surface morphology (parallel cylinders and perforated PI domains) occurred within 40 nm of the substrate, that is, within approximately one domain spacing of the substrate surface. Cross-sectional TEM of this sample showed three layers of structure (consistent with the initial film thickness of 3.0 × L_0) (see Figure 3b). The two layers closest to the free surface displayed lines consistent with parallel lamellae or parallel cylinders and perpendicular cylinders, and the layer closest to the substrate surface showed dots consistent with the ends of the parallel cylinders or the PS perforations of the PI domains identified by AFM. Thus, we have demonstrated the validity of the AFM/UVO etching approach, which is more quickly and easily implemented than cross-sectional TEM. AFM/UVO etching showed that, for all noninstantaneous solvent removal rates, the free surface morphology persisted through all but the last domain spacing of thickness (see Figure 3a, Figure 4d, and Figure S2 in the Supporting Information). Further, the featureless areas were not a purely surface phenomenon; therefore, we believe them to be kinetically trapped lamellar layers (*versus* a partial wetting layer of PI at the free surface) (see Figure 3a).

Because the free surface morphology propagated through the film but the substrate surface driving force for parallel cylinders also persisted, we were interested in how the morphology developed and extended from the free surface. For this investigation, we applied a 0.1 nm/min deswell rate to three samples, stopping at different swollen film thicknesses by instantaneously removing the remaining solvent from the film. The swollen film thicknesses corresponding to these points were 190 nm (5.1 × L_0, 41% solvent), 158 nm (4.3 × L_0, 29% solvent), or 125 nm (3.4 × L_0, 10% solvent) (see Figure 4a). We employed the AFM/UVO etching technique to better understand the morphology development during the solvent removal process (see Figure 4b–d). The AFM images from the film stopped at 190 nm showed that hexagonal ordering and thus reorientation of cylinders at the free surface was established early in the solvent removal process. However, this perpendicular cylinder morphology only existed through half of the film, and parallel cylinders became dominant at ≈60 nm from the substrate surface. Upon further solvent removal to 158 nm, the free surface morphology persisted until the last domain spacing of thickness (≈37 nm), though the substrate surface morphology appeared to have nonuniformly swollen domains. Finally, stopping the deswell at 125 nm resulted in even better order of the substrate surface morphology (see Figure 4d). Note that some featureless regions were found in the films stopped at the 158 and 125 nm swollen film thickness, as seen in the AFM images.

Proposed Reordering Mechanism. Our identification of morphology transformations as a function of solvent removal rate and characterization of the free surface morphology propagation through the film both suggest that fast deswell rates tend to produce parallel cylinders and that slower deswell rates promote perpendicular cylinder orientations. This conclusion is the opposite of that reached by Kim and Libera[28] who noted perpendicular orientations of cylinders in SBS films for fast solvent removal rates (~5 nL/s for a 1 cm^2 sample) and parallel orientations for slow solvent removal rates (~0.2 nL/s for a 1 cm^2 sample). The most significant difference between their study and ours

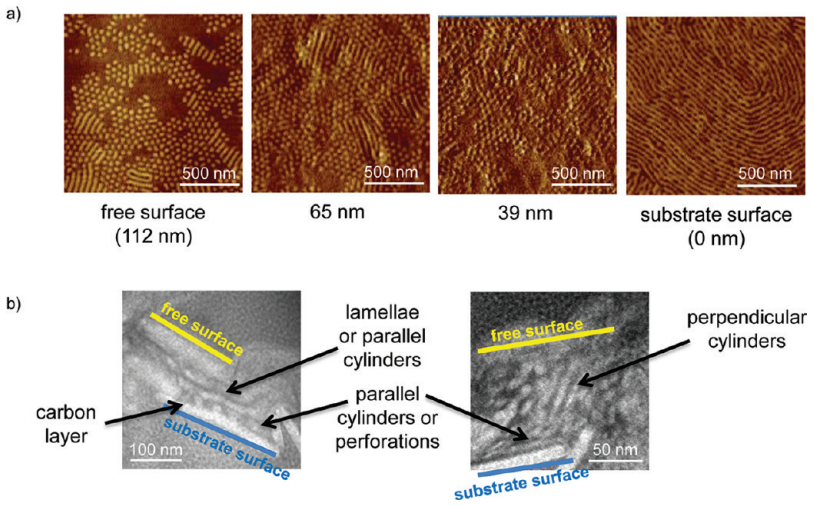

Figure 3. (a) AFM phase images of the through-film morphology of a dS-I-dS film annealed with chloroform vapor at a constant thickness for 2 h followed by solvent removal at a deswell rate of 0.5 nm/min. Images after each etching step were not necessarily taken at the same position on the sample. (b) Cross-sectional TEM image corresponding to the film in (a). The substrate surface and the free surface of the film are marked in blue and yellow, respectively. The sample was embedded in a disordered PS-*b*-PI block copolymer and stained with OsO_4 such that the dark regions of the film correspond to PI and the lighter regions correspond to dPS.

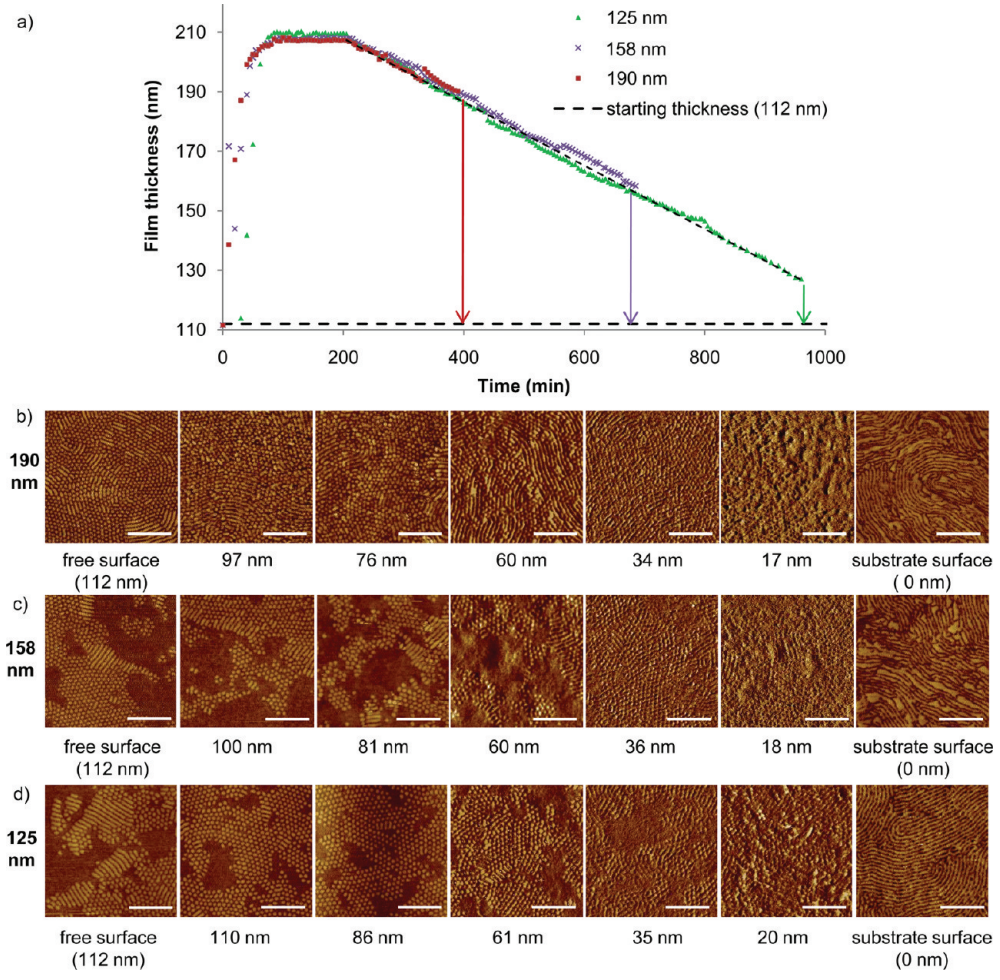

Figure 4. Morphology evolution of a film with a deswell rate of 0.1 nm/min. (a) Film thickness profiles for films annealed with chloroform vapor at a constant swollen thickness for 2 h followed by solvent removal at a deswell rate of 0.1 nm/min to different stopping film thicknesses. (b–d) AFM phase images corresponding to the annealing profiles in (a). Specifically, the anneals were stopped at swollen film thicknesses of (b) 190 nm, (c) 158 nm, and (d) 125 nm. Scale bars correspond to 500 nm. AFM images after each etching step were not necessarily taken at the same position.

was the initial film morphology upon initiation of solvent removal. Their study considered the morphology that formed upon casting from solution (*i.e.*, the film initially was disordered), whereas our study focused on starting from a post-SVA morphology (*i.e.*, the film initially had a well-ordered parallel cylinder morphology). Thus, the ordering mechanism for their system would have involved nucleation of the ordered morphology, whereas the mechanism in our system must involve changes to an existing morphology. We considered three possibilities for the promotion of perpendicular cylinders during slow solvent removal conditions. First, an effectively neutral free surface condition upon solvent evaporation would promote perpendicular cylinders at this surface;[12] however, if the chloroform vapor atmosphere provided a neutral free surface, we would have expected perpendicular cylinders to form during the 2 h hold at a constant swollen film thickness (see Figure 1). Second, the entropic penalty for forming a wetting layer of the lower surface tension PI block due to the ABA architecture of the dS-I-dS polymer could provide a driving force for stabilization of perpendicular cylinders,[36−38] but again, we would have expected this driving force to promote perpendicular rather than parallel cylinders during the hold at constant swollen film thickness. On the basis of these considerations, we propose a third scenario as the most plausible mechanism for reordering in our system: Initially, as solvent begins to evaporate, the film is subjected to an ever-changing commensurability condition as the film thickness (t), the nanostructure domain spacing of the swollen film (L), and the ratio t/L changes. To accommodate these changes, the parallel orientation would incur more energy penalties (in the form of chain stretching/compression or nucleation of islands/holes) compared with the perpendicular orientation. The ability of perpendicular orientations to accommodate incommensurability has been previously illustrated.[39] This reorientation of the cylinders can occur either by "flipping" of the parallel cylinders or by breakup and re-formation of cylinders with the new orientation. Literature precedent suggests that, in solvent vapor annealed systems, the latter is more common.[27] Figure 4 provides evidence of the perpendicular orientation propagating through the film as a front, and Figure 2 shows that the parallel orientation is maintained adjacent to the substrate surface. This evidence suggests that the re-formation mechanism is the likely route to reorientation in our system, as well.

Additionally, during breakup and re-formation of cylinders, lamellar PI layers could form and become kinetically trapped in the film for the 0.5 and 0.1 nm/min rates, whereas the slower 0.05 nm/min rate may provide time for these features to relax into the more thermodynamically favored cylinder structure (see Figure 2). Furthermore, the lack of featureless areas in the film subjected to the 0.1 nm/min deswell rate and stopped at 190 nm compared to the presence of featureless areas in films stopped at 158 and 125 nm (see Figure 4) suggests that the kinetics of featureless area formation should also be taken into account when considering how to eliminate such defects in cylinder-forming thin films. Additional work to monitor nanostructure development during the annealing process with a technique such as *in situ* grazing incidence small-angle X-ray scattering (GISAXS) as well as analysis of island/hole formation and possible elimination during solvent removal may further elucidate the self-assembly mechanism.

CONCLUSION

In summary, we systematically investigated the morphology development of a cylinder-forming dS-I-dS thin film as a function of solvent removal rate. To fully characterize the through-film morphologies and assess the degree to which the free surface morphology propagated through the film, we employed successive AFM/UVO etching steps, an approach that allowed us to characterize the films more easily and rapidly than was possible with cross-sectional TEM. The films formed well-ordered parallel cylinders upon exposure to a constant concentration of chloroform vapor (*i.e.*, constant swollen film thickness). This well-ordered morphology was trapped upon instantaneous solvent removal. Upon removing solvent very slowly (0.05 nm/min), the cylinders at the free surface reoriented perpendicular to the substrate surface, an effect that propagated through the film until the copolymer domain closest to the substrate surface. For intermediate solvent removal rates (0.5 nm/min, 0.1 nm/min), evolution of featureless regions, presumably parallel lamellae, occurred in addition to cylinder reorientation. Furthermore, comparison of films stopped at different points during the solvent removal process (0.1 nm/min deswell rate) provided evidence that cylinder reorientation propagated from the free surface through the film and toward the substrate as a front. These findings have important implications for the design and solution processing of nanostructured materials for nanotemplating and membrane (nanoporous and conducting) applications.

METHODS

Polymer Synthesis. The dS-I-dS block copolymer was synthesized *via* sequential anionic polymerization of perdeuterated styrene (d-styrene) (Acros, stabilized, 98+ atom% D) and isoprene (Acros, 98% stabilized) in cyclohexane (Fisher, degassed and purified using alumina and Q5 catalyst columns) at 40 °C under an argon environment. Perdeuterated styrene was used for the end blocks to facilitate additional thin film

characterization in the future *via* rotational small-angle neutron scattering (RSANS), a recently introduced technique for probing thin film morphology symmetry and orientation.[40] The polymerization was initiated with *sec*-butyllithium (Acros, 1.3 M in cyclohexane/*n*-hexane). Prior to synthesis, the isoprene and d-styrene monomers were degassed and purified by distillation over *n*-butyllithium (Acros, 2.5 M in hexane) and di-*n*-butylmagnesium (Acros, 0.5 M in heptane), respectively. The reaction was terminated using an acidic methanol solution, and the copolymer was precipitated in methanol, washed, and then freeze-dried from benzene. The final polymer had a number average molar mass of 160 kg/mol, a polydispersity index of 1.07, and block volume fractions of $f_{dS} = 0.10$, $f_I = 0.78$, and $f_{dS} = 0.12$ as determined from gel permeation chromatography (GPC) of aliquots taken during the synthesis. The bulk domain spacing was 37 nm as determined by small-angle X-ray scattering (SAXS).

Thin Film Annealing. Thin films were annealed with chloroform vapor using a setup in which nitrogen gas is bubbled through chloroform to produce a solvent-rich vapor stream that is combined with a pure nitrogen stream prior to entering the annealing chamber.[23,41,42] The relative flow rates of these streams were controlled with 0−50 mL/min volumetric flow meters to manipulate the vapor pressure of chloroform in the annealing chamber and thus control the swollen film thickness. The different deswell rates were achieved in the following manner: for instantaneous solvent removal, both flows were stopped, and the top of the annealing chamber was removed to facilitate fast solvent evaporation from the film into the atmosphere; for the 0.5 nm/min deswell rate, the annealing chamber was purged with nitrogen at a rate of 0.5 mL/min; for the 0.1 and 0.05 nm/min deswell rates, the flow of the chloroform rich stream was gradually reduced while holding the flow rate of the pure nitrogen stream constant. The top of the annealing chamber was quartz to facilitate *in situ* film thickness measurements with a Filmetrics F20-UV reflectance spectrometer. We accounted for changes in the film refractive index upon solvent vapor sorption when fitting reflectance spectra.[42]

UVO Etching. UVO etching was conducted in a Jelight Model 342 UVO cleaner in 5 s increments with the samples placed ≈1 cm from the lamp. Samples were soaked in filtered isopropyl alcohol (0.2 μm PTFE filter) for ≈5 min between exposures and dried under a stream of nitrogen. AFM images after each etching step were not necessarily taken at the same position on the sample.

Cross-Sectional TEM. Films were embedded in a disordered PI-*b*-PS copolymer and cryo-microtomed for cross-sectional imaging. Designating the free surface of the film as "Side 1" and the substrate surface of the film as "Side 2", the embedding procedure was a follows: First, the substrate-supported annealed film was carbon coated (≈10 nm) on Side 1. Next, a poly(acrylic acid) (PAA) solution in water (25 wt %, Acros Organics) was dropped on Side 1 and allowed to dry overnight at ≈50% humidity. The film was peeled from the substrate surface using a razor blade and tweezers, thus exposing Side 2. Side 2 was carbon coated (≈10 nm), and then a poly(isoprene-*b*-styrene) (PI-*b*-PS) embedding solution (11 kg/mol, $f_{PS} = 0.51$, 25 wt % polymer in *n*-hexane) was dropped on Side 2 and allowed to dry overnight. The PAA layer was removed from Side 1 by placing the film in water for ≈2−5 h. The film was allowed to dry under ambient conditions before proceeding to the next step. Another layer of carbon was coated on Side 1 (≈10 nm). The PI-*b*-PS solution was dropped on Side 1 and allowed to dry overnight. The sample was stored under vacuum until it was cut with the microtome. Thin sections (≈70 nm thickness) of the embedded sample were microtomed on a Leica Reichart Ultracut S microtome with a cryo attachment at −80 °C. The sections were stained with OsO_4 vapor for 15 min, which preferentially stains the poly(isoprene) domains of the block copolymers. TEM images were acquired on a JEOL JEM-2000FX TEM.

Acknowledgment. This paper was prepared under cooperative agreement 70NANB7H6178 from NIST, U.S. Department of Commerce. The statements, findings, conclusions, and recommendations are those of the authors and do not necessarily reflect the views of NIST or the U.S. Department of Commerce. This work was supported by the National Science Foundation (NSF) through an NSF CAREER grant, DMR-0645586, and an NSF Graduate Research Fellowship to J.N.L.A. W.-S.Y. was supported by the Department of Defense through AFOSR-PECASE (FA95 50-09-1-0706). J.R.S. was supported by the UD NSF REU Site Program (NSF EEC-0754348). We acknowledge the University of Delaware W. M. Keck Electron Microscopy Facility for use of their AFM and TEM facilities and the DuPont−Northwestern−Dow Collaborative Access Team (supported by E.I. DuPont de Nemours & Co., The Dow Chemical Company, and the State of Illinois) located at Sector 5 of the Advanced Photon Source for SAXS data. Use of the APS facility was supported by the U.S. Department of Energy, Office of Science, Office of Basic Energy Sciences, under Contract No. DE-AC02-06CH11357. We thank M. S. Tureau and S. M. Mastroianni for synthesis of the polymers used in this work, and Dr. J. E. Seppala for helpful discussion.

Supporting Information Available: Radial integration of FFT patterns from AFM images used to compare domain sizes at the free surface and substrate surface of annealed and as-cast films. UVO etching/AFM phase images corresponding a film prepared with a deswell rate of 0.05 nm/min. This material is available free of charge *via* the Internet at http://pubs.acs.org.

REFERENCES AND NOTES

1. Urade, V. N.; Wei, T. C.; Tate, M. P.; Kowalski, J. D.; Hillhouse, H. W. Nanofabrication of Double-Gyroid Thin Films. *Chem. Mater.* **2007**, *19*, 768–777.
2. Ruiz, R.; Kang, H.; Detcheverry, F. A.; Dobisz, E.; Kercher, D. S.; Albrecht, T. R.; De Pablo, J. J.; Nealey, P. F. Density Multiplication and Improved Lithography by Directed Block Copolymer Assembly. *Science* **2008**, *321*, 936–939.
3. Park, S.; Wang, J.-Y.; Kim, B.; Xu, J.; Russell, T. P. A Simple Route to Highly Oriented and Ordered Nanoporous Block Copolymer Templates. *ACS Nano* **2008**, *2*, 766–772.
4. Thurn-Albrecht, T.; Steiner, R.; DeRouchey, J.; Stafford, C. M.; Huang, E.; Bal, M.; Tuominen, M.; Hawker, C. J.; Russell, T. P. Nanoscopic Templates from Oriented Block Copolymer Films. *Adv. Mater.* **2000**, *12*, 787–791.
5. Olson, D. A.; Chen, L.; Hillmyer, M. A. Templating Nanoporous Polymers with Ordered Block Copolymers. *Chem. Mater.* **2008**, *20*, 869–890.
6. Yang, S. Y.; Ryu, I.; Kim, H. Y.; Kim, J. K.; Jang, S. K.; Russell, T. P. Nanoporous Membranes with Ultrahigh Selectivity and Flux for the Filtration of Viruses. *Adv. Mater.* **2006**, *18*, 709–712.
7. Phillip, W. A.; O'Neill, B.; Rodwogin, M.; Hillmyer, M. A.; Cussler, E. L. Self-Assembled Block Copolymer Thin Films as Water Filtration Membranes. *ACS Appl. Mater. Interfaces* **2010**, *2*, 847–853.
8. Segalman, R. A.; McCulloch, B.; Kirmayer, S.; Urban, J. J. Block Copolymers for Organic Optoelectronics. *Macromolecules* **2009**, *42*, 9205–9216.
9. Joo, W.; Park, M. S.; Kim, J. K. Block Copolymer Film with Sponge-like Nanoporous Structure for Antireflection Coating. *Langmuir* **2006**, *22*, 7960–7963.
10. Bates, F. S. Polymer−Polymer Phase-Behavior. *Science* **1991**, *251*, 898–905.
11. Matsen, M. W.; Thompson, R. B. Equilibrium Behavior of Symmetric ABA Triblock Copolymer Melts. *J. Chem. Phys.* **1999**, *111*, 7139–7146.
12. Albert, J. N. L.; Epps, T. H., III. Self-Assembly of Block Copolymer Thin Films. *Mater. Today* **2010**, *13*, 24–33.
13. Kelly, J. Y.; Albert, J. N. L.; Howarter, J. A.; Kang, S.; Stafford, C. M.; Epps, T. H.; Fasolka, M. J. Investigation of Thermally Responsive Block Copolymer Thin Film Morphologies Using Gradients. *ACS Appl. Mater. Interfaces* **2010**, *2*, 3241–3248.
14. Di, Z.; Posselt, D.; Smilgies, D.-M.; Papadakis, C. M. Structural Rearrangements in a Lamellar Diblock Copolymer Thin Film during Treatment with Saturated Solvent Vapor. *Macromolecules* **2010**, *43*, 418–427.
15. Sun, Y.; Henderson, K. J.; Jiang, Z.; Strzalka, J. W.; Wang, J.; Shull, K. R. Effects of Reactive Annealing on the Structure of Poly(methacrylic acid)-Poly(methyl methacrylate) Diblock Copolymer Thin Films. *Macromolecules* **2011**, *44*, 6525–6531.

16. Cavicchi, K. A.; Berthiaume, K. J.; Russell, T. P. Solvent Annealing Thin Films of Poly(isoprene-*b*-lactide). *Polymer* **2005**, *46*, 11635–11639.
17. Xuan, Y.; Peng, J.; Cui, L.; Wang, H.; Li, B.; Han, Y. Morphology Development of Ultrathin Symmetric Diblock Copolymer Film *via* Solvent Vapor Treatment. *Macromolecules* **2004**, *37*, 7301–7307.
18. Zettl, U.; Knoll, A.; Tsarkova, L. Effect of Confinement on the Mesoscale and Macroscopic Swelling of Thin Block Copolymer Films. *Langmuir* **2010**, *26*, 6610–6617.
19. Knoll, A.; Horvat, A.; Lyakhova, K. S.; Krausch, G.; Sevink, G. J. A.; Zvelindovsky, A. V.; Magerle, R. Phase Behavior in Thin Films of Cylinder-Forming Block Copolymers. *Phys. Rev. Lett.* **2002**, *89*, 035501.
20. Jung, Y. S.; Ross, C. A. Solvent-Vapor-Induced Tunability of Self-Assembled Block Copolymer Patterns. *Adv. Mater.* **2009**, *21*, 2540–2545.
21. Bang, J.; Kim, B. J.; Stein, G. E.; Russell, T. P.; Li, X.; Wang, J.; Kramer, E. J.; Hawker, C. J. Effect of Humidity on the Ordering of PEO-Based Copolymer Thin Films. *Macromolecules* **2007**, *40*, 7019–7025.
22. Li, Y.; Huang, H.; He, T.; Gong, Y. The Effect of the Preferential Affinity of the Solvent on the Microstructure of Solution-Cast Block Copolymer Thin Films. *J. Phys. Chem. B* **2010**, *114*, 1264–1270.
23. Cavicchi, K. A.; Russell, T. P. Solvent Annealed Thin Films of Asymmetric Polyisoprene-Polylactide Diblock Copolymers. *Macromolecules* **2007**, *40*, 1181–1186.
24. Kim, G.; Libera, M. Kinetic Constraints on the Development of Surface Microstructure in SBS Thin Films. *Macromolecules* **1998**, *31*, 2670–2672.
25. Phillip, W. A.; Hillmyer, M. A.; Cussler, E. L. Cylinder Orientation Mechanism in Block Copolymer Thin Films upon Solvent Evaporation. *Macromolecules* **2010**, *43*, 7763–7770.
26. Peng, J.; Kim, D. H.; Knoll, W.; Xuan, Y.; Li, B.; Han, Y. Morphologies in Solvent-Annealed Thin Films of Symmetric Diblock Copolymer. *J. Chem. Phys.* **2006**, *125*, 064702.
27. Paik, M. Y.; Bosworth, J. K.; Smilges, D.-M.; Schwartz, E. L.; Andre, X.; Ober, C. K. Reversible Morphology Control in Block Copolymer Films *via* Solvent Vapor Processing: An *In Situ* GISAXS Study. *Macromolecules* **2010**, *43*, 4253–4260.
28. Kim, G.; Libera, M. Morphological Development in Solvent-Cast Polystyrene-Polybutadiene-Polystyrene (SBS) Triblock Copolymer Thin Films. *Macromolecules* **1998**, *31*, 2569–2577.
29. Fukunaga, K.; Elbs, H.; Magerle, R.; Krausch, G. Large-Scale Alignment of ABC Block Copolymer Microdomains *via* Solvent Vapor Treatment. *Macromolecules* **2000**, *33*, 947–953.
30. Elbs, H.; Drummer, C.; Abetz, V.; Krausch, G. Thin Film Morphologies of ABC Triblock Copolymers Prepared from Solution. *Macromolecules* **2002**, *35*, 5570–5577.
31. Fasolka, M. J.; Harris, D. J.; Mayes, A. M.; Yoon, M.; Mochrie, S. G. J. Observed Substrate Topography-Mediated Lateral Patterning of Diblock Copolymer Films. *Phys. Rev. Lett.* **1997**, *79*, 3018–3021.
32. Epps, T. H.; DeLongchamp, D. M.; Fasolka, M. J.; Fischer, D. A.; Jablonski, E. L. Substrate Surface Energy Dependent Morphology and Dewetting in an ABC Triblock Copolymer Film. *Langmuir* **2007**, *23*, 3355–3362.
33. Stafford, C. M.; Roskov, K. E.; Epps, T. H.; Fasolka, M. J. Generating Thickness Gradients of Thin Polymer Films *via* Flow Coating. *Rev. Sci. Instrum.* **2006**, *77*, 023908.
34. Chow, T. S. Molecular Interpretation of the Glass Transition Temperature of Polymer-Diluent Systems. *Macromolecules* **1980**, *13*, 362–364.
35. Park, M.; Harrison, C.; Chaikin, P. M.; Register, R. A.; Adamson, D. H. Block Copolymer Lithography: Periodic Arrays of $\sim 10^{11}$ Holes in 1 Square Centimeter. *Science* **1997**, *276*, 1401–1404.
36. Khanna, V.; Cochran, E. W.; Hexemer, A.; Stein, G. E.; Fredrickson, G. H.; Kramer, E. J.; Li, X.; Wang, J.; Hahn, S. F. Effect of Chain Architecture and Surface Energies on the Ordering Behavior of Lamellar and Cylinder Forming Block Copolymers. *Macromolecules* **2006**, *39*, 9346–9356.
37. Kubo, T.; Wang, R. F.; Olson, D. A.; Rodwogin, M.; Hillmyer, M. A. Spontaneous Alignment of Self-Assembled ABC Triblock Terpolymers for Large-Area Nanolithography. *Appl. Phys. Lett.* **2008**, *93*, 133112.
38. Vu, T.; Mahadevapuram, N.; Perera, G. M.; Stein, G. E. Controlling Domain Orientations in Thin Films of AB and ABA Block Copolymers. *Macromolecules* **2011**, *44*, 6121–6127.
39. Huang, E.; Mansky, P.; Russell, T. P.; Harrison, C.; Chaikin, P. M.; Register, R. A.; Hawker, C. J.; Mays, J. Mixed Lamellar Films: Evolution, Commensurability Effects, and Preferential Defect Formation. *Macromolecules* **2000**, *33*, 80–88.
40. Zhang, X.; Berry, B. C.; Yager, K. G.; Kim, S.; Jones, R. L.; Satija, S.; Pickel, D. L.; Douglas, J. F.; Karim, A. Surface Morphology Diagram for Cylinder-Forming Block Copolymer Thin Films. *ACS Nano* **2008**, *2*, 2331–2341.
41. Knoll, A.; Magerle, R.; Krausch, G. Phase Behavior in Thin Films of Cylinder-Forming ABA Block Copolymers: Experiments. *J. Chem. Phys.* **2004**, *120*, 1105–1116.
42. Albert, J. N. L.; Bogart, T. D.; Lewis, R. L.; Beers, K. L.; Fasolka, M. J.; Hutchison, J. B.; Vogt, B. D.; Epps, T. H. Gradient Solvent Vapor Annealing of Block Copolymer Thin Films Using a Microfluidic Mixing Device. *Nano Lett.* **2011**, *11*, 1351–1357.